remote sensing

MDPI

Article

Study on Morphometrical Urban Aerodynamic Roughness Multi-Scale Exploration Using LiDAR Remote Sensing

Seung Man An [1,*], Byungsoo Kim [2], Chaeyeon Yi [3], Jeong-Hee Eum [4], Jung-Hun Woo [5] and Wolfgang Wende [6,7]

[1] Housing & Real Estate Research Division, Korea Research Institute for Human Settlements, Sejong 30149, Republic of Korea
[2] TENELEVEN Inc., Seoul 03925, Republic of Korea; kimby@1011.co.kr
[3] Research Center for Atmospheric Environment, Hankuk University of Foreign Studies, Yongin 17035, Republic of Korea; prpr2222@hufs.ac.kr
[4] Department of Landscape Architecture, Kyungpook National University, Daegu 41566, Republic of Korea; eumjh@knu.ac.kr
[5] Graduate School of Environmental Studies, Seoul National University, Seoul 08826, Republic of Korea; woojh21@snu.ac.kr
[6] Leibniz Institut für Ökologische Raumentwicklung, 01217 Dresden, Germany; w.wende@ioer.de
[7] TUD Dresden University of Technology for Urban Development, 01062 Dresden, Germany
* Correspondence: sm_an@krihs.r.kr; Tel.: +82-44-960-0307 (ext. 30147)

Abstract: This study proposes the use of light detection and ranging (LiDAR) remote sensing (RS) to support morphometric research for estimating the aerodynamic roughness length (z_0) of building placement on various scales. A LiDAR three-dimensional point cloud (3DPC) data processing graphical user interface (GUI) was developed to explore the z_0 and related urban canopy parameters (UCPs) in the Incheon metropolitan area in South Korea. The results show that multi-scale urban aerodynamic roughness exploration is viable and can address differences in urban building data at various spatial resolutions. Although validating morphological multi-scale UCPs using dense tall towers is challenging, emerging low-cost and efficient methods can serve as substitutes. However, further efforts are required to link the measured z_0 to building form regulations, such as floor area ratio, and expand RS research to obtain more quantitative and qualitative knowledge.

Keywords: building placement; aerodynamic roughness length (z_0); urban canopy parameters (UCPs); morphometric method; observational method; multi-scale exploration; light detection and ranging (LiDAR); three-dimensional point cloud (3DPC)

check for updates

Citation: An, S.M.; Kim, B.; Yi, C.; Eum, J.-H.; Woo, J.-H.; Wende, W. Study on Morphometrical Urban Aerodynamic Roughness Multi-Scale Exploration Using LiDAR Remote Sensing. *Remote Sens.* **2024**, *16*, 2418. https://doi.org/10.3390/rs16132418

Academic Editor: Ashraf Dewan

Received: 26 April 2024
Revised: 15 June 2024
Accepted: 27 June 2024
Published: 1 July 2024

Copyright: © 2024 by the authors. Licensee MDPI, Basel, Switzerland. This article is an open access article distributed under the terms and conditions of the Creative Commons Attribution (CC BY) license (https://creativecommons.org/licenses/by/4.0/).

1. Introduction

Interest in environmental planning for sustainable futures in densely populated areas such as metropolitan cities is increasing [1–3]. Major countries and cities worldwide are aiming to develop low-carbon societies and implement a national spatial data infrastructure (NSDI), which applies digital mapping as an important resource [4]. Several scholars have used digital maps and geographic information system (GIS) applications to identify and monitor the spatial expansion of built-up urban environments. Such applications measure the horizontal and vertical expansion of urban building clusters using various indicators, such as urban canopy parameters (UCPs), and thus are being extensively explored by meteorologists in conjunction with continuous observations of intra-urban winds [5,6].

The "mean urban wind" concept [7] is relatively new and depends on long-term urban climate studies [8,9]. Notably, building placement is an important factor to consider under this concept. Through empirical analyses of building placement and wind distribution observations, the aerodynamic roughness of cities can be reliably quantified [10,11], thereby promoting the development of enhanced numerical weather prediction models that focus

on urban forms [12–14]. Urban climate planners are interested in and use these morphological techniques to describe the relationship between building placement and wind flows, with the goal of harmonizing these methods during urban development [15–17]. Thus, a method of exploring urban forms on different scales is required. However, few studies on morphometrics related to aerodynamic roughness or similar indicators have thoroughly considered such methods [18–22]. Additionally, many studies use manually drawn digital building footprints, which are mostly generalized based on map scales. These manual methods restrict the flexible scaling of morphometric approaches, thereby limiting their applicability across various scales.

Recently, the use of light detection and ranging (LiDAR) remote sensing (RS) spatial data and technologies in various applications for large urban areas has been discussed as an alternative to adopting a multi-scale approach [23–25]. Note that through aerial and satellite- and mobile-based applications, LiDAR RS can support rapid and detailed detection and provide information related to urban building placement changes [26]. However, a method capable of identifying building placement or shape using LiDAR three-dimensional point cloud (3DPC) data has not yet been developed. This issue needs to be addressed to facilitate the implementation of multi-scale morphometric evaluations.

Therefore, this study aimed to develop an approach for processing LiDAR 3DPC data to explore aerodynamic roughness and related parameters on various scales. Notably, the methodology and results of this study are primarily based on the use of a graphical user interface (GUI) developed to process LiDAR 3DPC data.

2. Materials and Methods

As cities expand, the spatial arrangements of urban buildings become increasingly diverse, thereby complicating the interpretation of ventilation functions. Furthermore, given that individual buildings can significantly affect the ventilation dynamics in urban areas, the placement of all buildings must be considered. Therefore, this study proposes a methodology capable of measuring all buildings within an urban area using airborne LiDAR 3DPC data. The use of the morphometric methodology to measure the influence of buildings on wind distribution has been extensively studied [10,27,28] and widely employed to estimate the wind profile within the urban boundary layer (UBL). This method assumes minimal wake interference and applies a logarithmic velocity profile for winds approaching obstacles.

2.1. Input Data

The classified airborne LiDAR 3DPC dataset constructed by the National Geographic Information Institute (NGII) in South Korea was the primary dataset used for this study. The NGII has surveyed all urban areas of South Korea twice and will continue surveying urban areas as part of a digital twin plan that is based on spatial data [25]. The 3DPC dataset was acquired as a part of the National Airborne Laser Scanning Project, which is a component of the NGII survey program. The classification of building 3DPCs was conducted based on an understanding of the reflective properties of active light and the associated urban morphological attributes, and it contains data procured through rule-based automatic and manual classification processes and quality assessments and quality control (QA/QC) performed by the NGII. Additionally, supplementary data, such as building-related digital and land-use maps and automatic weather station (AWS) measurement data, were used. Table 1 lists the datasets used in the study.

Table 1. Data used in this study.

Data	Provider	Property Applied
Airborne LiDAR 3DPC	NGII	Classified building and ground 3DPCs [25]
Automatic Weather Station	KT	Air temperature and relative humidity [29]
Digital Photograph (Ortho)	NGII	Image at 0.25 m resolution for visual interpretation
Land Use (Zone)	NGII	Land use (zone code) [30]
Digital Map (Building)	NGII	Building coverage area and floor area [30]

Abbreviations: Three-dimensional point cloud (3DPC); National Geographic Information Institute (NGII); Korea Telecommunications (KT). Note: NGII [30] offers a list of downloadable geospatial information for free; however, LiDAR data are not included. To use LiDAR data for evaluation purposes, contact the Smart Spatial Information Division, NGII (Email: ngii2018@korea.kr, Tel: +82-31-210-2700). For use of AWS data, visit the AirMapKorea website (https://iot.airmapkorea.kt.com/info/, accessed on 26 June 2024).

2.2. Methods

Building morphology is one of the main topics in urban climate planning and urban design studies because building placement not only determines the urban skyline but also influences both external and internal wind flows in urban spaces [18]. A well-known indicator for quantifying this effect on external and internal flows is aerodynamic roughness length (z_0), which is based on the atmospheric boundary layer theory governing the turbulence intensity between building placement and air. Quantification approaches can be categorized into [10] observational methods (Figure 1a), which are dynamic techniques that rely on wind or turbulence measurement data and are based on Monin–Obukhov similarity theory, and morphological methods (Figure 1b), which quantify z_0 based on the shape characteristics of the buildings [10,11]. Note that the atmospheric interaction between each urban building setting and the local wind flow is unique and observations require tall towers and instrumentation; thus, urban building morphology is a more advantageous parameter for application and dissemination. Therefore, we developed morphological methods to quantify z_0 to enable multi-scale surveillance and extensive urban building placement exploration.

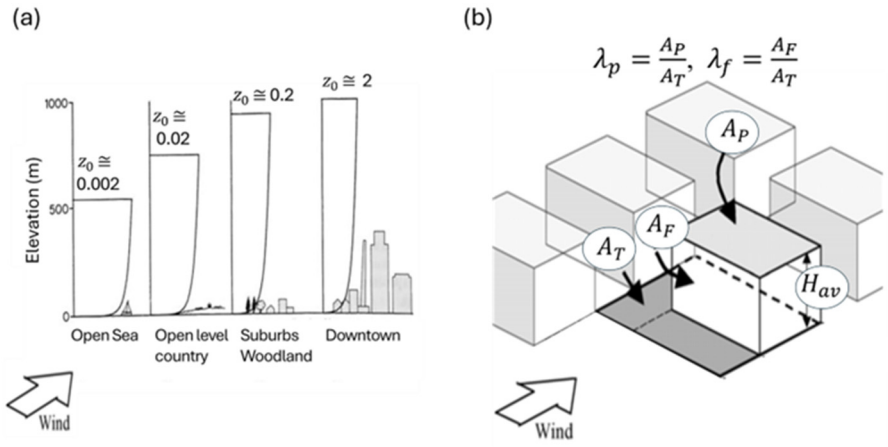


Figure 1. Two urban mean wind speed estimation methods. (**a**) Observational method, which assumes that neutral atmospheric stratification winds follow logarithmic wind law at a H_{av} above the surface [13]; (**b**) morphological method, which can determine the urban mean wind-related value without requiring tall towers and instrumentation [10].

Numerous studies have developed empirical models based on urban morphology to estimate z_0 and interpret complex and heterogeneous building placements [27,28,31–35]. Moreover, many morphological studies have utilized digital building footprint maps to assess the influence of building morphology on the average wind distribution [18–22]. The size and shape of buildings have been measured and include parameters such as the building average height (H_{av}), as well as plane area (λ_p) and frontal area (λ_f) roughness [28]. How-

ever, although digital maps provide higher accuracy in building footprint classification, the shape and area of manually drawn digital building footprints are significantly dependent on the applied map scale. Therefore, we used the 3DPC building-class sampling method proposed by Yi and An [24]. The primary and core methodological distinction of the present study lies in the estimation of z_0, which is based on the building LiDAR 3DPCs.

The following measurements for H_{av}, λ_p, and λ_f differ from the methods employed by previous scholars. In practice, a user-specified rectangular grid size termed the lot area (A_T) and a lot of the same area divided into subgrids have been applied as variables, as shown in equation (1). We assumed that each subgrid contains a building without identification error when it covers 1 m^2 (1 m × 1 m), and this assumption is applied to all grids. From the measurement framework, the ratio of building placement coverage in a grid area (A_T) is defined as λ_p, which can be measured as follows:

$$\lambda_p = \frac{A_P}{A_T}, \tag{1}$$

where A_T is the size of the lot area of the specified grid and A_P is the detected building placement footprint area in the specified grid. A_P can be measured as follows:

$$A_P = \sum_{i=1}^{n} A_S \cdot \rho(\mathrm{x_I},\ \mathrm{y_i}), \tag{2}$$

where A_S is the size of the subgrid area and $\rho(\mathrm{x_i},\ \mathrm{y_i})$ is a function that can detect the presence of building 3DPC in the subgrid area (A_S). This function was obtained using the following formula:

$$\rho(\mathrm{x_i},\ \mathrm{y_i}) = \begin{cases} 1\ if\ any\ building\ 3DPC\ exists\ in\ a\ subgrid\ area\ (\mathrm{x_i},\ \mathrm{y_i}) \\ 0\ \text{otherwise} \end{cases} \tag{3}$$

Similarly, λ_f, which represents the ratio of buildings placement frontal area in a grid area, can be measured as follows:

$$\lambda_f = \frac{A_F}{A_T}, \tag{4}$$

where A_F is the detected building placement frontal area facing the wind perpendicularly in the specified grid. To compute λ_f, we first project the building 3DPC to the rz-plane, which is orthogonal to the wind direction. Then, we apply a method similar to that used to compute the frontal area A_F, which can be measured as follows:

$$A_F = \sum_{i=1}^{n} \sqrt{A_S} \cdot \max_{1 \le j \le m} h(\mathrm{r_i}, \mathrm{z_j}) \tag{5}$$

$$h(\mathrm{r_i}, \mathrm{z_j}) = \begin{cases} \mathrm{z_j}\ if\ any\ building\ 3DPC\ exists\ in\ a\ subgrid\ area\ (\mathrm{r_i},\ \mathrm{z_j}) \\ 0\ \text{otherwise} \end{cases}, \tag{6}$$

where n and m represent the effective resolution of the specified grid in the r and z directions, respectively. Building average height (H_{av}) refers to the average height of a group of individual mean height of subgrids and is calculated by summing all subgrid mean heights from the ground to building top and dividing the value by the total number of identified building subgrids. Building maximum height (H_{max}) is determined by selecting the highest value from all subgrid max building heights. Each subgrid max building height is also determined by selecting the highest value from all 3DPCs from the ground. Then, the LiDAR 3DPC data-driven building average height (H_{av}), building maximum height (H_{max}), plane area index (λ_p), and frontal area index (λ_f) values were applied as UCPs according to the equations in Table 2 (Figure 2).

Table 2. Methods of calculating the aerodynamic roughness length (z_0) used in this study.

Method	z_0 Estimation Equation and Description
MacDonald [28]	$Mac_z_d = \left[1 - \alpha^{-\lambda_p} \cdot (\lambda_p - 1)\right] \cdot H_{av}$ $Mac_z_0 = \left(1 - \frac{z_d}{h_{av}}\right) exp\left[-\left\{0.5\beta \cdot \frac{C_d}{k^2}\left(1 - \frac{Z_d}{h_{av}}\right) \cdot \lambda_f\right\}^{-0.5}\right] \cdot H_{av}$ κ is the von Karman constant (0.4); C_d is the drag coefficient (1.2); α is the constant in displacement height expression (4.43 for the staggered arrays); and β is the sheltering effect factor (1.0)
Kanda [33]	$Kan_z_d = \left[c_0 \cdot X^2 + \left(a_0 \lambda_p^{b_0} - c_0\right) X\right] \cdot H_{max}$ $Kan_z_0 = \left(b_1 \cdot Y^2 + bc_1 \cdot Y + a_1\right) \cdot Mac_z_0$ H_{std} is the standard deviation of building height; H_{av} is the average building height; H_{max} is the maximum building height; a_0, b_0, c_0, a_1, b_1, and c_1 denote the regressed constant parameters, with values of 1.29, 0.36, −0.17, 0.71, 20.21, and −0.77; and z_0 (mac) represents the z_0 value obtained using the MacDonald [28] method

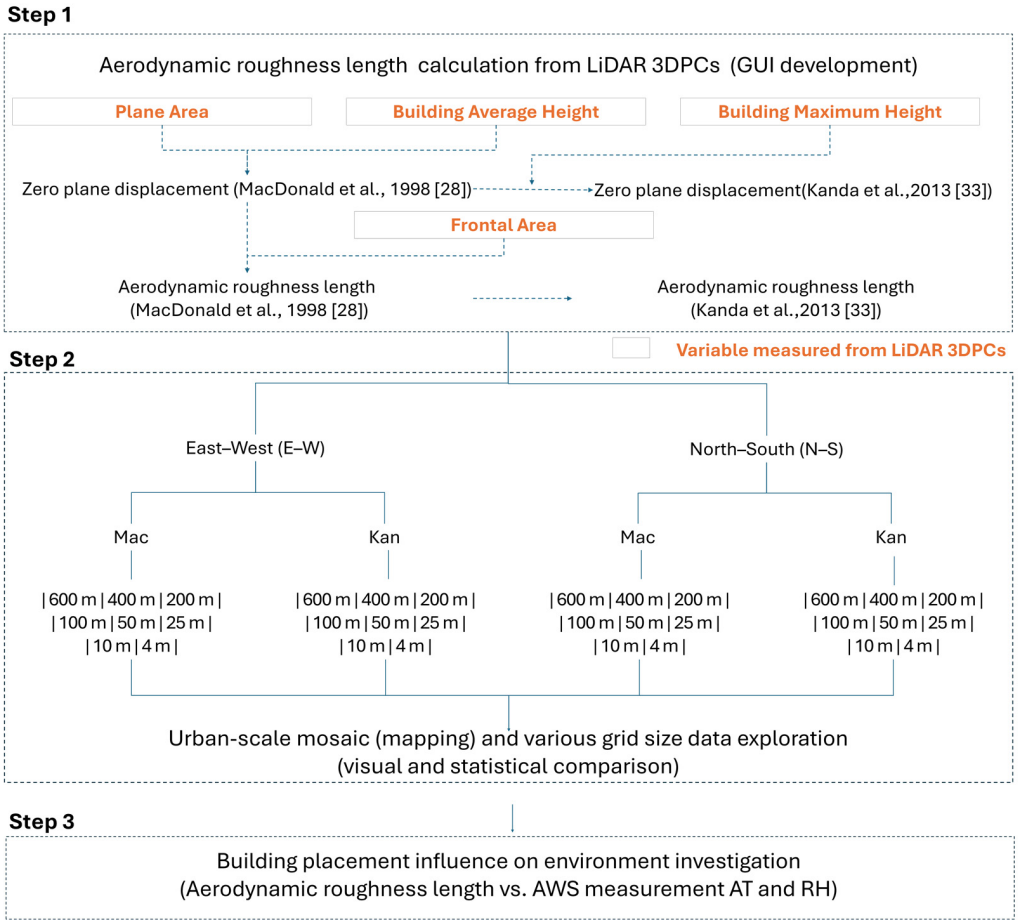


Figure 2. Workflow for the proposed multi-scale exploration approach. Abbreviations: three-dimensional point cloud (3DPC), graphical user interface (GUI), automatic weather station (AWS), air temperature (AT), relative humidity (RH).

Figure 2 shows the three steps and a detailed workflow. The GUI proposed and developed by An [25] was modified to include a function for measuring the morphometric aerodynamic roughness. In step 1, four variables (H_{max}, H_{av}, λ_p, and λ_f) associated with roughness elements are directly measured from LiDAR 3DPCs and then sequentially applied to determine the displacement height (z_d) and aerodynamic roughness length (z_0). In step 2, eight grid sizes (600, 400, 200, 100, 50, 20, 10, and 4 m), two estima-

tion methods [28,33], and two wind-direction (east–west (E–W) and north–south (N–S)) case-based z_0 values were mapped for multi-scale exploration. These maps were either compared with each other or with external data (such as land-use maps). In step 3, the potential influence of current building placement on urban environment is investigated. Air temperature (AT) and relative humidity (RH) data from the AWS observation network are compared with the z_0 values.

2.2.1. Study Area

Incheon metropolitan area is an optimized study area for analyzing the impact of urban-scale building placement, which was also the target area for An's (2023) sky view factor (SVF) analysis [25]. Situated in northwestern South Korea, Incheon borders the Seoul and Gyeonggi provinces. According to an analysis of meteorological data conducted by the Korea Meteorological Agency for the development of wind resource maps, the annual average wind speed in Incheon is 3.9 m/s, and the prevailing wind direction is northwest. Baengnyeongdo predominantly experiences westerly winds, whereas northwesterly winds are more common at the Incheon International Airport. Notably, Sudogwon (Seoul, Gyeonggi-do, and Incheon) is a dense AWS-monitoring testbed.

The study area covered 501.5 km^2 and encompassed half of Incheon's administrative area (1062.63 km^2). In this region, although numerous buildings have been developed, urban buildings are still being constructed. According to digital maps (building footprint) from the NGII, buildings with 1–5 floors in the region cover 42.9 km^2 of land area and have a total floor area of 242.9 km^2, constituting 88.1 and 51.8% of the total land area and floor area, respectively. According to South Korean building regulations, structures exceeding 30 floors are classified as high-rise buildings, whereas those exceeding 50 floors are categorized as super high-rise buildings [36]. In the study region, buildings spanning 11–29 floors represent only 7.8% of the total building coverage area but account for 36.1% of the total floor area, with the majority of these being used as residential buildings (Figure 3 and Table 3).

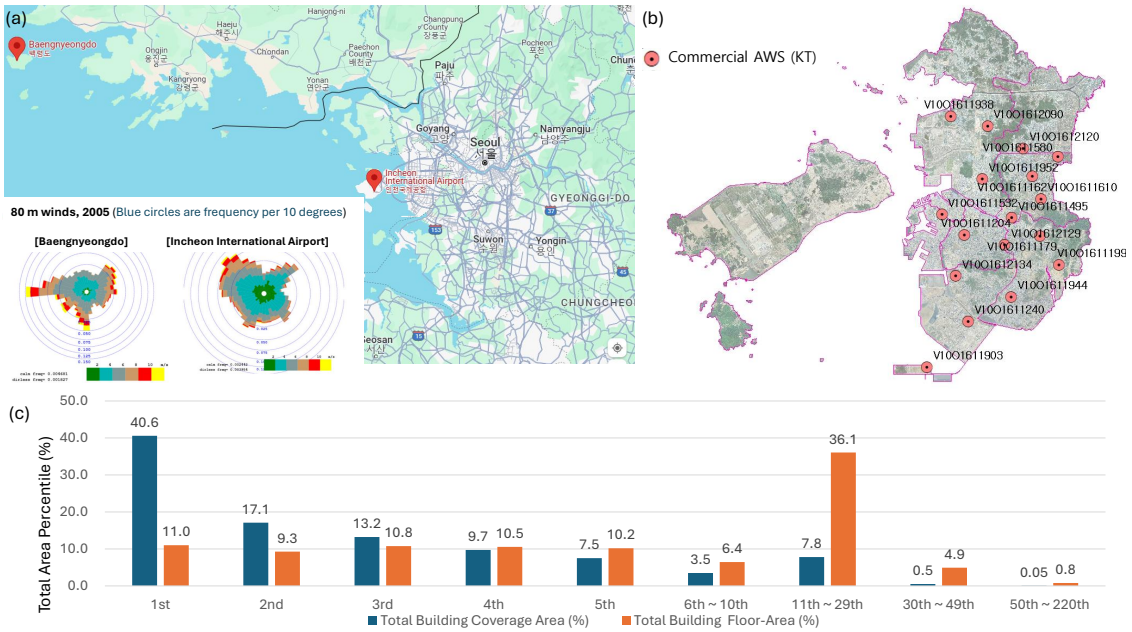


Figure 3. Prevailing wind conditions and statistical building placement in the study area. (**a**) Prevailing winds at measurement locations (Baengnyeongdo and the Incheon International Airport), with wind rose charts. (**b**) Commercial air temperature and relative humidity observation at the AWS locations in the study area. (**c**) Differences in the statistical percent mean between the total building coverage and floor area according to the floor area class.

Table 3. Building coverage area and building floor area statistics for the study region.

Floor	Count (ea.)	Coverage (m^2)	Total Building Coverage (10,000 m^2)	Total Building Coverage (%)	Mean Building Floor-Area (m^2)	Total Building Floor-Area (10,000 m^2)	Total Building Floor-Area (%)
1	162,618	121.5	1976.0	40.6	364.5	5928.1	11.0
2	44,002	189.2	832.5	17.1	1135.2	4995.1	9.3
3	26,870	239.4	643.4	13.2	2155.0	5790.6	10.8
4	19,854	238.3	473.2	9.7	2859.8	5677.8	10.5
5	11,007	331.8	365.2	7.5	4977.0	5478.1	10.2
6~10	3111	547.4	170.3	3.5	11,155.1	3470.4	6.4
11~29	5493	691.8	380.0	7.8	35,355.5	19,420.8	36.1
30~49	274	906.0	24.8	0.5	96,685.1	2649.2	4.9
50~220	16	1395.8	2.2	0.0	266,742.3	426.8	0.8
			4867.7	100.0		53,836.8	100.0

Note: The table was generated from the NGII Digital Map (Building) [30] and used both the building coverage area and number of floors. Buildings with 1–5 floors constitute 88.1% of the total building coverage and 51.8% of the total building floor area.

2.2.2. 3DPC GUI Development and Single Building Scale Data Exploration

Qt and Microsoft Foundation Class libraries were used to develop the functionality required to measure the roughness length and ensure GUI integration [37]. The input/output development for the 3DPC format (LAS) was based on the laser specification version 1.4-R15, based on the American Society for Photogrammetry and Remote Sensing (ASPRS) [38]. Quick 3DPC measurement visualization and functional integration are available in Qt as it provides a cross-platform application programming framework for non-GUI as well as GUI applications. Then, using the developed GUI, LiDAR 3DPC data for a single building at 100 × 100 m were explored based on the z_0 and relevant UCPs as sample records.

2.2.3. Aerodynamic Roughness Exploration of the Urban-scale Mosaic and Various Grid Sizes

The urban area is so large that optimization processes such as dividing and reuniting are inevitable. Hence, we introduced the mosaic method proposed by An [25] to maintain both a wide coverage and detailed exploration in urban aerodynamic roughness and relevant UCPs. We obtained 750 3DPC building files at a size of 1200 × 1200 m and grouped them as inputs for the batch processing of z_0, and UCP measurements were then performed. All data input/output operations were adjusted using a GUI prompt (xy-plane grid manipulation I/O window of Figure 4b). The derivation of z_0 from the 3DPC dataset involved the following experimental tests: (1) wind direction, (2) z_0 estimation, and (3) grid (A_T) size. Determining the prevailing wind direction is important when quantifying building placement influences, such as z_0, and the z_0 results for the N–S and E–W directions were quantitatively compared per square grid (A_T). Additionally, the results of MacDonald et al. [28] and Kanda [33] were compared. Lastly, to analyze the spatial distribution of z_0 values affected by the differences in the grid (A_T) size, we applied matrixes of 2 × 2 (600 m), 3 × 3 (400 m), 6 × 6 (200 m), 12 × 12 (100 m), 24 × 24 (50 m), 60 × 60 (20 m), 120 × 120 (10 m), and 300 × 300 (4 m). Within the GUI workbench, the data for each of the 750 files, which were aligned with the coordinates referenced by the raster settings, were allocated to the corresponding grid matrix. The GUI workbench, which is organized within directories, sequentially produced the American Standard Code for Information Interchange (ASCII) [39] raster data for the UCPs (such as λ_p, λ_f, H_{av}, H_{max}, z_d, and z_0 subdirectories).

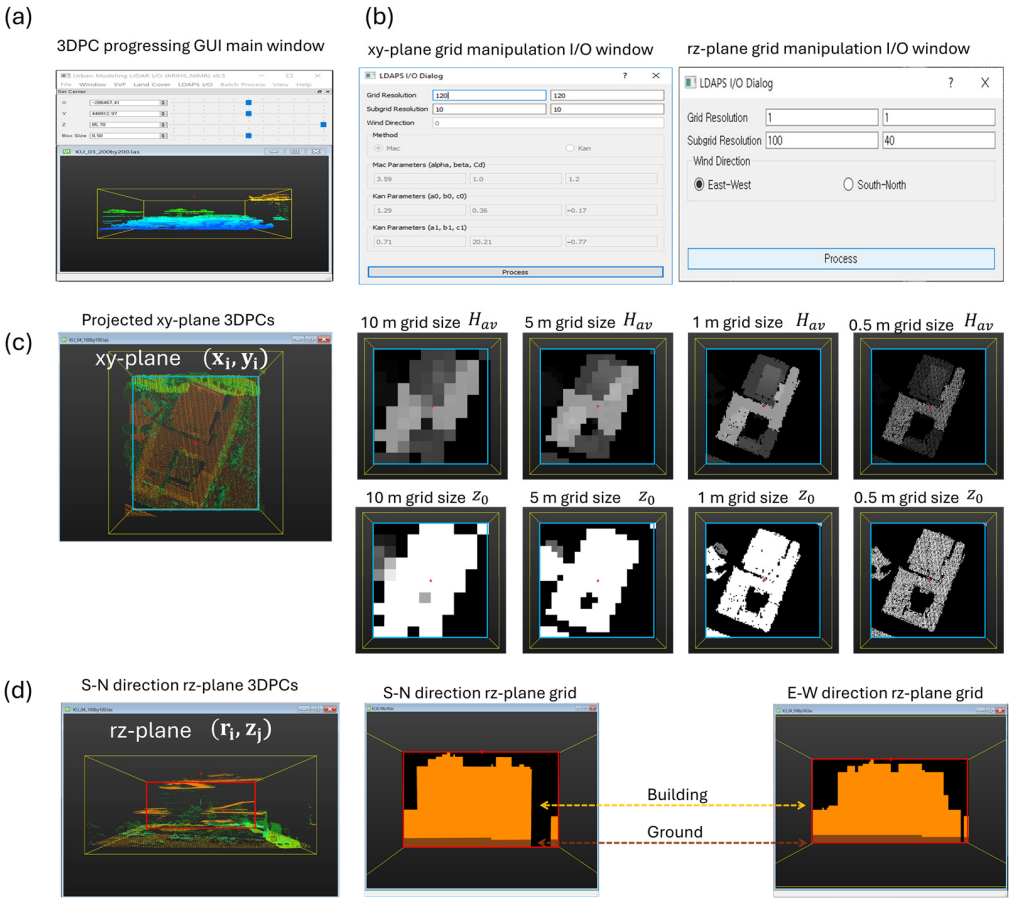


Figure 4. Single-building scale 3DPC and aerodynamic roughness exploration. (**a**) Main GUI for exploring visualized LiDAR 3DPCs; (**b**) I/O window for experimental settings; (**c**) xy-plane projection of building 3DPCs and horizontally measured multi-scale H_{av} and z_0; and (**d**) rz-plane projection of building 3DPCs and vertically measured λ_f (S–N wind and E–W wind).

Then, the mosaic process was performed using the Python script-based Environmental Systems Research Institute (ESRI) ArcGIS spatial functions (raster mosaic). Subsequently, the areas outside the study region were eliminated from the mosaic maps, and visual and statistical comparisons were conducted for the buildings in the study area.

After the mosaic and mapping, we explored a set of z_d and z_0 spatial mosaic-image data visually and statistically. Whole map datasets were divided into five classes (quintiles) for visual comparison of the spatial distribution of the two parameters. Specifically, to portray how z_0 differed with the wind direction (blowing from the N–S versus the E–W directions), a simple map overlay deviation method was applied. The deviation map for two different wind directions (E–W and N–S) was overlaid on a land-use map to discern the hotspots and quantify the differences across the study area.

2.2.4. Investigation of Building Placement Influence on the Environment

Unfortunately, the morphometric measurement results were difficult to verify due to the absence of a nearby flux tower to obtain data for the logarithmic wind-speed profile drawing. However, in South Korea, information technology (IT) companies such as Korea Telecommunications (KT) are expanding and densifying automatic weather observation (AWS) networks in Sudogwon and commercializing the collected weather data.

Therefore, we aimed to use these observation data to validate the quantified z_0 and explore the connection between current urban building placements and climate influences. This is done by comparing the morphometric z_0 with pedestrian-level AT and RH data. The AT and RH observation data from KT for 1 June–31 August 2018 were used. Hourly

observed AT and RH values from the 17 AWS during the study period were averaged to obtain the representative weather characteristics. The average AT, RH, and Dif_{Mac_z0} values of the 17 AWS were spatially explored. Lastly, 17 AWS location based UCPs (Mac_{zd}, Kan_{zd}, Mac_{z0}, Kan_{z0}) were explored to find a cautious scale issues when developing connection between urban building placements and climate influences. Although the method cannot directly verify urban mean wind, it can support indirectly describing benefits of building placement management on urban climate adaptation.

3. Results

3.1. Single Building Scale 3DPC and Aerodynamic Roughness Map Exploration

The 100 × 100 m-sized LiDAR 3DPC data sample effectively depicts the shapes of single building and a strong relationship with quantified z_0 or relevant UCPs. As shown in Figure 4, measuring z_0 and relevant UCPs requires not only horizontal xy-plane calculations but also vertical rz-plane calculations depending on the wind direction. Based on an evaluation of 3DPC and raster visualization data, we gained an understanding of the spatial characteristics of the input data and designed appropriate grid and subgrid output options for urban-scale exploration.

3.2. Urban-Scale Mosaic and Various Grid Size Map Exploration

The first insight gained from exploring the multi-scale urban roughness length was how visual porosity changes with different grid sampling sizes. Visual interpretation of porosity areas can provide clues about urban roughness if we assume that wind flows follow connected porosity areas. The results show an increase in porosity area as the grid size becomes finer. Conversely, as the resolution becomes coarser, the porosity area (white) is shown as clumped areas (red). Overall, porosity is more noticeable in z_0 maps than in z_d maps. As shown in Figure 5, the measurement method (e.g., Mac_{Z0} vs. Kan_{Z0}) did not cause a significant visual difference, although changing the grid size from 4 m to 600 m did cause a difference. This trend is consistent in both the z_d and z_0 maps. However, a slight visual difference due to the measurement method was found, and it was more noticeable in the z_d maps because the building's maximum height (H_{max}) was used in Kan_{zd}. A higher spatial variation of z_d was observed by Kan_{zd} than by Mac_{zd}, especially at the 400 m grid size (Figure 5a). On the other hand, the z_0 visual differences due to measurement methods were insignificant, except Kan_{z0}, which appears to be slightly thicker than Mac_{z0} (Figure 5b). Despite many visual interpretations, it is difficult to identify a single map from Figure 5 that best represents on-site porosity or aerodynamic conditions, either quantitatively or qualitatively.

Therefore, we compared the Mac_{z0} map with grid sizes ranging from 4 to 600 m to aerial photographs with scales of 1:1000–1:100,000, assuming that the photos better represented in situ conditions. As shown in Figure 5c, when the grid sizes have sufficient building resolving power, such as 4 and 10 m, the porosity between buildings is discernible. However, when the grid size exceeds 20 m and loses this resolving power, porosity identification shifts to the level of land cover or districts. The best 'Mac_{z0}-aerial photograph' map pair varies with each grid size, necessitating adjustments in interpretation focus and visual targets. Given all this information, using multiple scales is necessary to understand urban aerodynamic roughness from different visual perspectives and to develop better strategies.

Obtaining statistical exploration results is simpler than performing the relatively difficult and complex visual exploration of z_0 and relevant UCPs. Additionally, assuming that maintaining a consistent UCP value is important and beneficial for methodological application and dissemination, Table 4 and Figure 6 provide guidance for selecting the proper UCP. When observing the variations in the mean values with increasing grid size, H_{max} showed a noticeable increase, while λ_f showed a considerable decrease (Figure 6a). Furthermore, λ_p showed a slight decrease, while H_{av} showed an increase. With respect to maximum values, as the grid size increased, H_{av} decreased and λ_f exhibited an exponential decreasing trend. The standard deviation (std) trend was quite similar to the mean. Hence,

λ_p and λ_f are quite unsuitable for spatial analysis application because they are extremely sensitive to changes in grid size. Moreover, the results show that Mac_{zd} is an appropriate measurement method because the Kan_{zd} mean is also quite sensitive and led to higher mean, maximum, and std values than Mac_{zd} while producing similar trends with increasing grid size (Figure 6b).

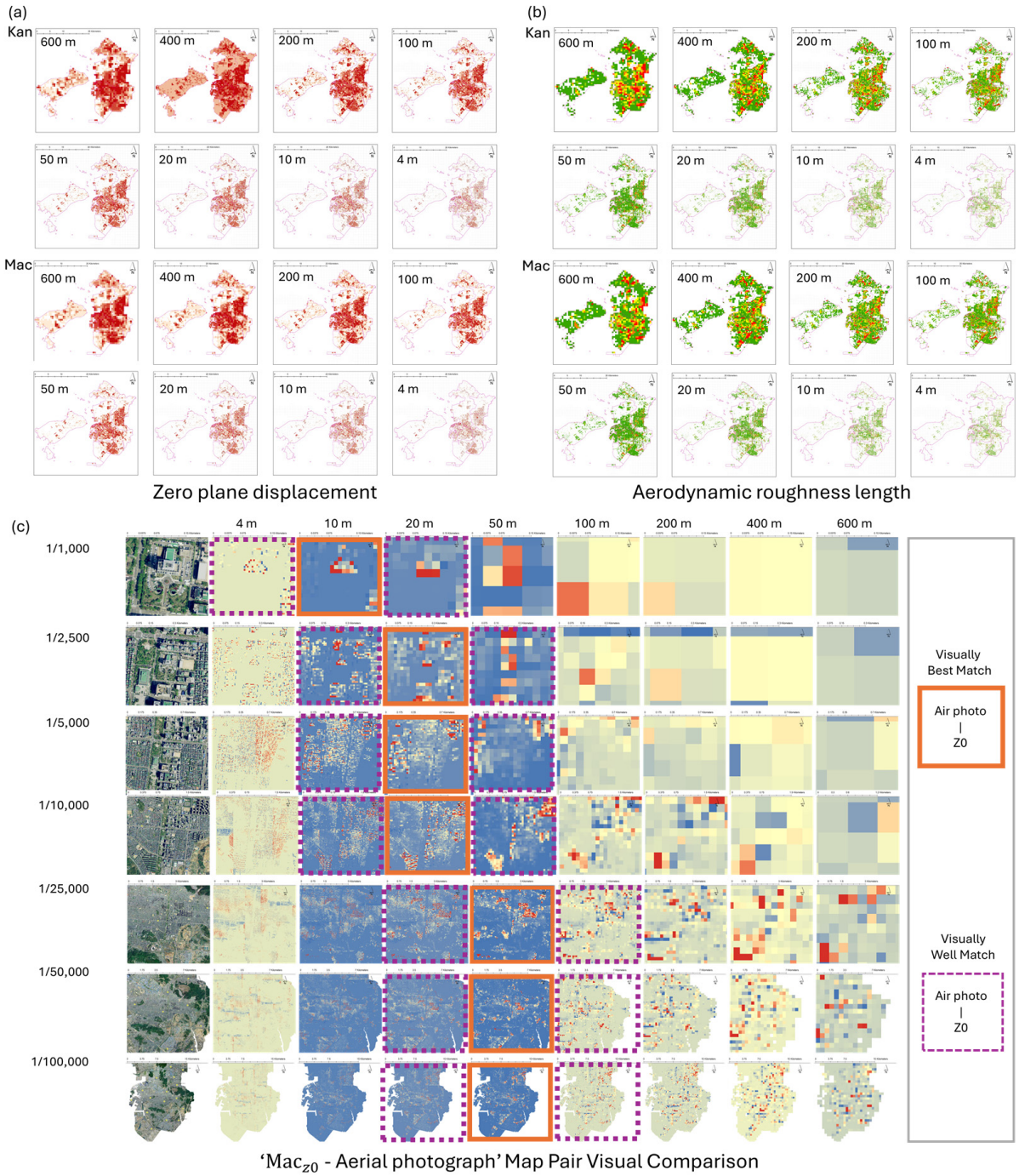


Figure 5. Visual comparisons of z_d and z_0 generated from the LiDAR 3DPC for various grid sizes (E–W wind direction). (**a**) z_d generated for eight grid sizes (4, 10, 25, 50, 100, 200, 400, and 600 m) using two estimation methods; (**b**) z_0 generated for eight grid sizes (4, 10, 25, 50, 100, 200, 400, and 600 m) using two estimation methods [28,33]; (**c**) comparison of Mac_{z0}(4–600 m) and aerial photograph map (scale = 1:1000–1:100,000) shows the visually best-matched and well-matched 'Mac_{z0} grid size-aerial photograph scale'.

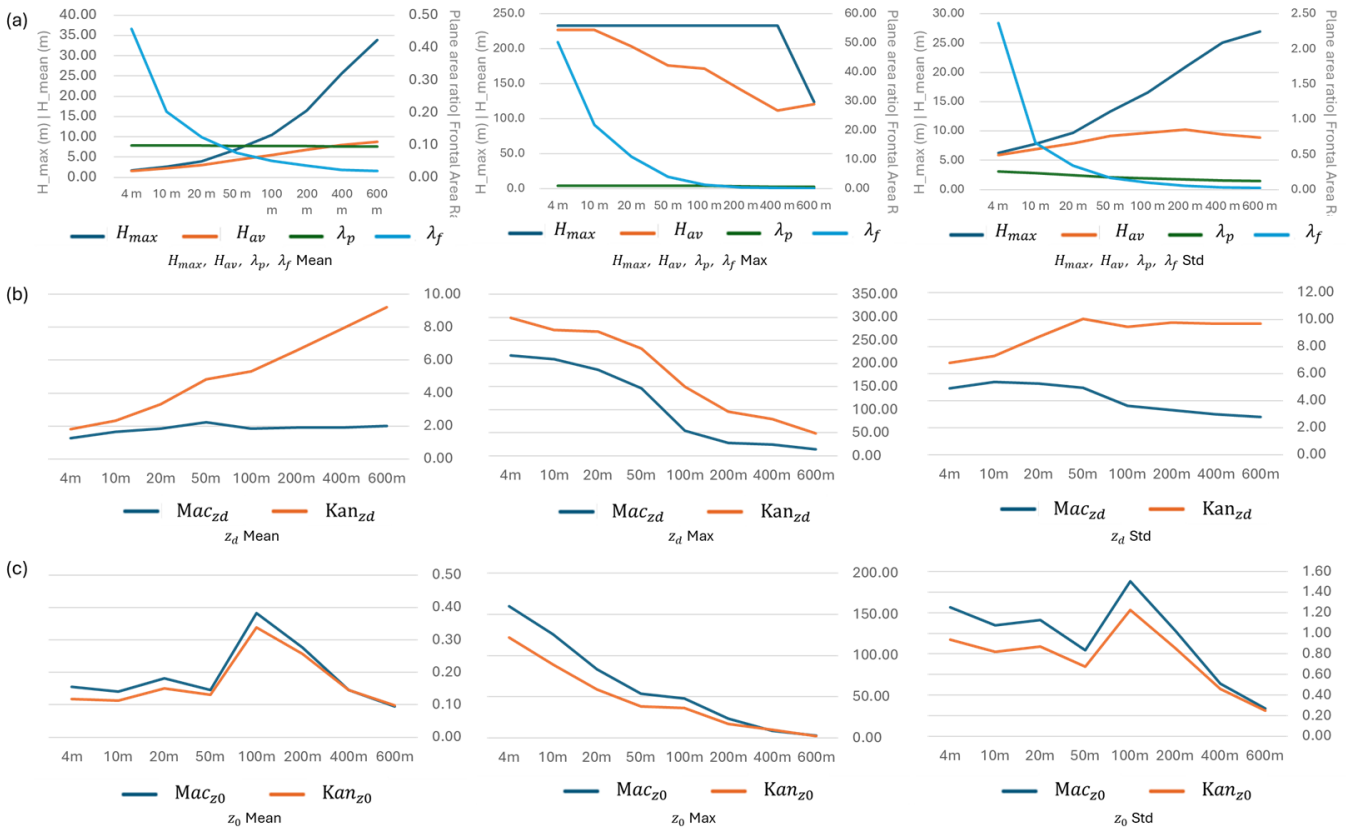


Figure 6. Statistical comparison of the mean, maximum (max), and standard deviation (std) values of building maximum height (H_{max}), average height (H_{av}), plane area (λ_p), frontal area (λ_f), displacement height (z_d), and aerodynamic roughness length (z_0) for different grid resolutions (E–W wind direction). (**a**) H_{av}, λ_p and λ_f values were analyzed for eight grid sizes (4, 10, 25, 50, 100, 200, 400, and 600 m). (**b**) z_d values estimated using the two methods [11] showed variations. (**c**) z_0 values estimated using the two methods [28,33].

Of note, z_0 is the most suitable UCP for spatial analysis applications because it is insensitive to changes in grid size (Figure 6c). Thus, it showed limited variations while Mac_{z0} presented slightly higher values than Kan_{z0} in terms of the mean, max, and std. However, for z_0, the mean also increases sharply at grid sizes of 200 m (0.26–0.28) and 100 m (0.34–0.38) compared to the values at other sizes (0.09–0.18).

Even with limitations in multi-scale data analyses and practical knowledge, the morphometric z_0 results can be useful for estimating current land use from an urban aerodynamic roughness perspective. Thus, current land use can be quantified using z_0. The land-use types in the study area are mainly associated with environmental conservation (UQA430), followed by residential use (UQA122 and UQA123), and heavy chemical polluting industry (UQA310) (Table 5). Figure 7 shows the land-use zones and the average value of each land use for each wind direction at the 50 m grid size (Mac_{z0} and Kan_{z0}). A large difference in the z_0 values measured for the E–W and N–S wind directions was detected in high-rise residential land-use areas (UQA123), which may represent zones of major interest for morphometric character analysis according to building placement to obtain better urban aerodynamic roughness values. Both the Mac and Kan methods exhibited the highest z_0 mean values for residential areas (UQA123) under the prevailing wind direction (E–W).

Table 4. Statistical mean, maximum (max), and standard deviation (std) values of building maximum (H_{max}) and average (H_{av}) roughness-element heights, plane area (λ_p), frontal area (λ_f), displacement height (z_d), and aerodynamic roughness length (z_0) for different grid resolutions (E–W wind direction) using the two methods [28,33].

Type	Grid (m)	H_{max}	H_{av}	λ_p	λ_f	Mac_{zd}	Kan_{zd}	Mac_{z0}	Kan_{z0}
Max	600	123.50	121.16	0.57	0.14	14.83	48.60	2.79	2.13
	400	232.97	111.83	0.61	0.28	24.67	80.27	8.71	10.01
	200	232.97	141.22	0.88	0.48	28.42	96.22	23.36	16.98
	100	232.65	171.69	0.97	1.29	55.02	149.89	47.63	36.12
	50	232.65	176.35	0.99	4.15	146.01	232.72	53.73	38.08
	20	232.65	203.39	1.00	11.03	186.18	268.96	83.25	59.04
	10	232.65	226.59	1.00	21.85	209.04	272.39	125.84	89.34
	4	232.65	226.63	1.00	50.31	217.63	299.00	159.92	122.01
Mean	600	33.89	8.83	0.09	0.02	2.02	9.23	0.09	0.10
	400	25.60	7.94	0.09	0.02	1.92	7.91	0.15	0.14
	200	16.44	6.78	0.10	0.04	1.90	6.59	0.28	0.26
	100	10.53	5.46	0.10	0.05	1.84	5.32	0.38	0.34
	50	6.98	4.36	0.10	0.07	2.22	4.83	0.15	0.13
	20	3.99	3.02	0.10	0.12	1.85	3.32	0.18	0.15
	10	2.68	2.26	0.10	0.20	1.64	2.33	0.14	0.11
	4	1.75	1.62	0.10	0.46	1.26	1.83	0.16	0.12
Std	600	26.98	8.85	0.12	0.02	2.80	9.69	0.27	0.25
	400	25.07	9.43	0.13	0.03	2.99	9.68	0.51	0.46
	200	20.89	10.20	0.14	0.06	3.28	9.77	1.02	0.85
	100	16.56	9.68	0.16	0.10	3.62	9.44	1.50	1.22
	50	13.31	9.18	0.17	0.17	4.96	10.05	0.84	0.68
	20	9.70	7.85	0.21	0.34	5.26	8.71	1.13	0.87
	10	7.79	6.84	0.23	0.67	5.38	7.31	1.08	0.82
	4	6.24	5.90	0.26	2.37	4.90	6.80	1.25	0.94

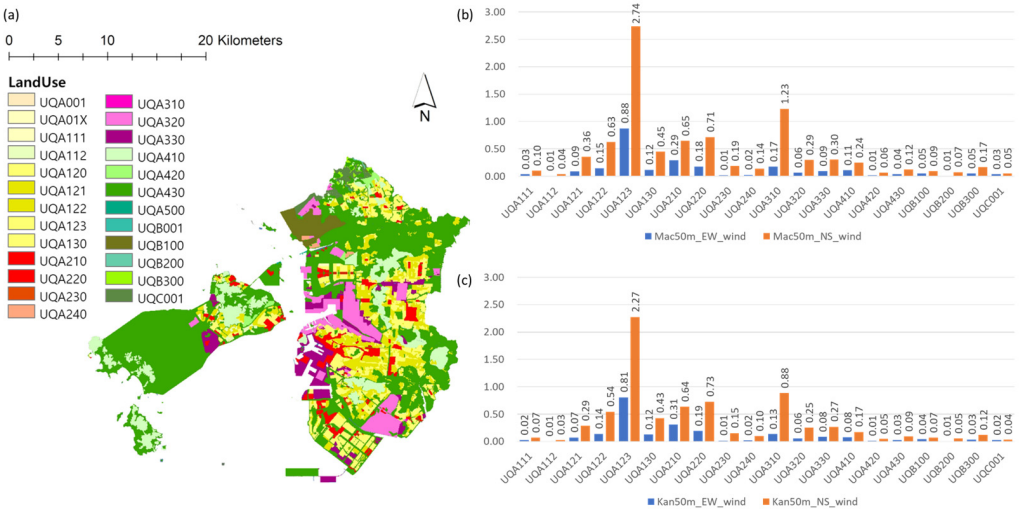


Figure 7. Differences in the aerodynamic roughness length (z_0) mean values due to wind direction for each land-use zone in the study area. (**a**) Land-use zoning code and map. (**b**) Difference in the statistical Mac_{z0} and (**c**) Kan_{z0} mean values for the E–W and N–S wind directions according to the land-use zone code. The land-use zone codes are explained in Table 5.

Table 5. Differences in the aerodynamic roughness length (z_0) mean values based on the wind direction for each land-use zone in the study area.

Code	Land-Use Purpose (Building)	Grid Area (%)	Mac_{z0}/50 m Grid			Kan_{z0} /50 m Grid		
			E–W	N–S	DIF	E–W	N–S	DIF
UQA111	Protect residential environments for independent housing	0.25	0.03	0.10	−0.06	0.02	0.07	−0.05
UQA112	Protect residential environments for multi-unit housing	0.39	0.01	0.04	−0.03	0.01	0.03	−0.02
UQA121	Create convenient residential environments for low-floor housing	2.85	0.09	0.36	−0.27	0.07	0.29	−0.21
UQA122	Create convenient residential environments for mid-floor housing	8.57	0.15	0.63	−0.48	0.14	0.54	−0.41
UQA123	Create convenient residential environments for mid/high housing	9.11	0.88	2.74	−1.87	0.81	2.27	−1.46
UQA130	Provide commercial environments to residential areas	3.73	0.12	0.45	−0.33	0.12	0.43	−0.30
UQA210	Expand commercial functions in the center/sub-center	0.76	0.29	0.65	−0.36	0.31	0.64	−0.32
UQA220	Provide general commercial and business functions	3.95	0.18	0.71	−0.54	0.19	0.73	−0.53
UQA230	Supply daily necessities and services in the neighboring area	0.08	0.01	0.19	−0.17	0.01	0.15	−0.14
UQA240	Increase the circulation function in the city and between areas	0.07	0.02	0.14	−0.11	0.02	0.10	−0.08
UQA310	Heavy chemical polluting industry	0.01	0.17	1.23	−1.05	0.13	0.88	−0.75
UQA320	Industries that are not environmentally friendly	7.13	0.06	0.29	−0.23	0.06	0.25	−0.19
UQA330	Light and other industries	5.04	0.09	0.30	−0.21	0.08	0.27	−0.18
UQA410	Protect natural green areas in the city	9.51	0.11	0.24	−0.14	0.08	0.17	−0.10
UQA420	Reserves for agricultural production	0.70	0.01	0.06	−0.05	0.01	0.05	−0.03
UQA430	Secure green space and future city sites	46.26	0.04	0.12	−0.08	0.03	0.09	−0.06
UQB100	Incorporate into future urban areas	0.05	0.05	0.09	−0.04	0.04	0.07	−0.03
UQB200	Reserves for agriculture and forests	0.04	0.01	0.07	−0.07	0.01	0.05	−0.05
UQB300	Protected areas	0.21	0.05	0.17	−0.12	0.03	0.12	−0.08
UQC001	Protect forests and promote agriculture	1.29	0.03	0.05	−0.02	0.02	0.04	−0.01

Notably, the differences in z_0 values between the E–W and N–S directions revealed the buildings in the land-use zones that are sensitive to wind direction. For example, as shown in Figure 7b,c, buildings in certain land-use types, such as UQA123, have a greater impact on z_0 when winds blow from the N–S direction. The z_0 value differences between E–W and N–S for industrial areas with heavy chemical and polluting industries (UQA310) were the second highest (−0.75 to −1.05). However, since these areas only account for 0.01% of the land use, their influence on overall wind flow in the study area is insignificant. Thus, further exploration was conducted to identify which roughness elements of building placement in the UQA123 land-use area influenced the differences in z_0 value between the E–W and N–S directions.

Figure 8 spatially explains the reason for the significant z_0 value differences between the E–W and N–S directions in the UQA123 land-use area. The map in Figure 8a shows the z_0 deviation spatial patterns in the two-wind direction overlaid with two types of land

use: high-rise residential (UQA123) and heavy chemical polluting industry (UQA310). The area covered by UQA123 is large, while the area covered by UQA310 is quite small. The map legend color changes to red when the majority of buildings are placed with their windward walls facing N–S, and it changes to blue when the majority of buildings are placed with their windward walls facing E–W. Several discernible hotspot areas, which are marked in red, can be observed in the eastern inland area of the study region. Figure 8b magnifies one of the red spots and visually matches it with aerial photographs. In the semi-transparent overlay image, most buildings are over twenty stories high, and their windward walls are facing N–S. Of note, the E–W-oriented long rectangular apartment buildings are associated with traditional Korean residential culture and represent a preferred residential type [40]. Because of the preference for sunny, south-facing residential buildings in South Korea, many areas designated as UQA123 include high-rise apartment buildings facing south. This trend is ongoing and is expected to continue for some time; thus, it not only changes the urban scenery but also influences the aerodynamic roughness and climatical adaptability of the city. Fortunately, the dominant wind patterns in the study region exhibit an easterly direction during summer and a northerly direction during winter (Figure 3a), thus conforming to the characteristic seasonal wind regimes influenced by the Siberian high-pressure system (during winter) and the East Asian monsoon (during summer) over the Korean Peninsula. Therefore, the morphometry of buildings in the hotspot area appears to be urban climate adaptive, thus providing not only effective urban wind preservation but also maintaining a cool environment in summer and a warm environment in winter.

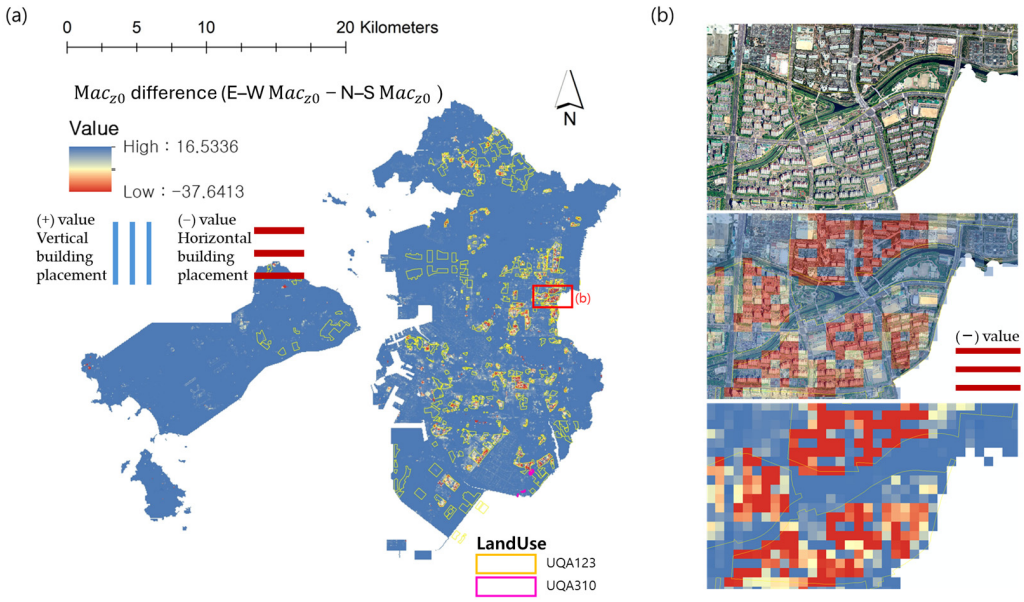


Figure 8. Aerial photograph based on an in-depth investigation of the high-rise residential zone (UQA123). (**a**) Map portraying the planned high-rise residential zone (UQA123) and the spatial distribution difference of Mac_{z0} based on 50 m grid size raster data. In the Mac_{z0} difference map, (+) values mean vertical building placement, and (−) values mean horizontal building placement. (**b**) In the visual comparison, red spots indicate areas where building placement-induced Mac_{z0} is significantly different between the E–W and N–S wind directions.

3.3. Relationship between Current Urban Building Placements and Climate Influences

Assuming each of the 17 AWS locations is surrounded by unique building placements and that AT and RH monitoring are seamlessly integrated, the average AT and RH values over 1862 h during the study period (1 June–31 August) can reliably represent the summer climate of each location. As shown in Figure 9, the average AT and RH values from the 17 AWS locations represent a typical coastal climate and are inversely related: when AT increases, RH decreases (see the regression curve in Figure 9b). Moreover, the relationship

between the z_0 difference and RH is stronger than that between the z_0 difference and AT (see Figure 9c,d). In other words, RH is more sensitive to building placement in terms of the prevailing wind direction, making it an efficient monitoring indicator. Because a lower RH (%) in summer is achieved by sites with better ventilation, RH can be used to monitor or control the impact of building placement. However, RH monitoring needs to be strictly controlled because, in the case of v16011903 (Figure 9e), other factors such as trees or soil have a greater influence than building placement.

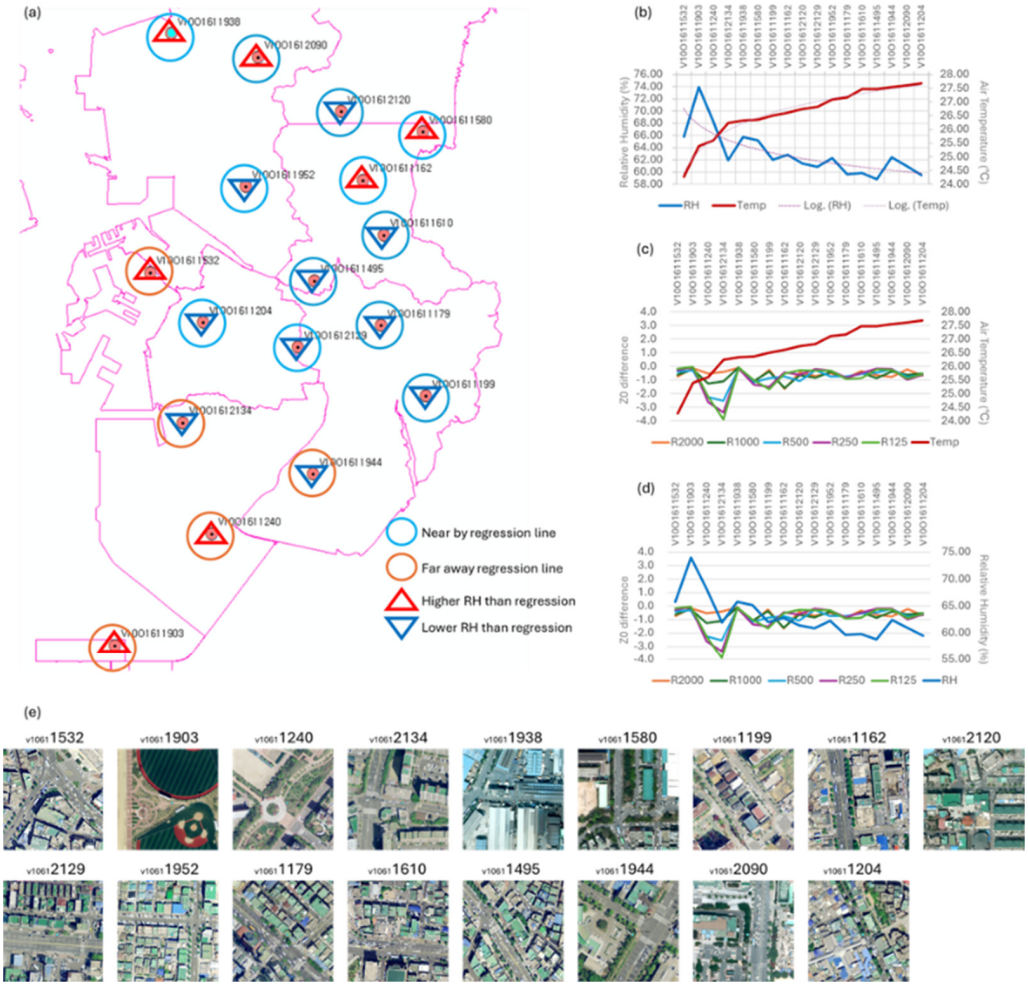


Figure 9. Differences in the average AT (°C), RH (%), and z_0 observations (for the E–W vs. N–S wind directions) recorded at the 17 AWSs. (**a**) AWS illustration of the spatial distribution and difference between RH observations and the regression. (**b**) Relationship between the mean AT and RH in summer (1 June –31 August 2018). (**c**) Relationships between the mean AT and averaged z_0-difference (E–W vs. N–S wind directions). (**d**) Relationships between the mean RH and averaged z_0 difference. The z_0 difference is averaged from various size circles (2000, 1000, 500, 250, and 125 m, denoted as R2000, R1000, R500, R250, and R125, respectively). (**e**) 1:1000 scale ortho photos of 17 AWS stations (center) surrounding building placement environments.

Table 6 shows the relationship between current urban building placements and climate influences. All z_0 difference values are negative, meaning that AWSs are located on buildings that have their windward walls facing N–S (see Figure 8a). Of note, the majority of negative z_0 difference values decrease as the radii of the averaging circle decreases from 2000 to 125 m. This suggests that the influence of buildings on urban climate can vary depending on the scale of the survey, such as a larger macro-scale or a smaller micro-scale.

In addition, we should also consider that Mac_{z0} quantification results can be affected not only by site-specific building placement but also by adjustments to the analysis grid size and search radius. Figure 10 shows that the overall Mac_{z0} mean, std, minimum (min), and maximum (max) graphs showed trends similar to those in Figure 6c, with each of the 17 AWS locations showing unique trends. The mean Mac_{z0} of the 17 AWS locations is relatively stable at a search radius of R2000 but becomes more variable as the search radius decreases. Moreover, using a very large search area (e.g., R2000) often generalizes the aerodynamic roughness of the site, while using a very small search area (e.g., R125) can inappropriately reduce the number of samples, thereby decreasing the statistical reliability.

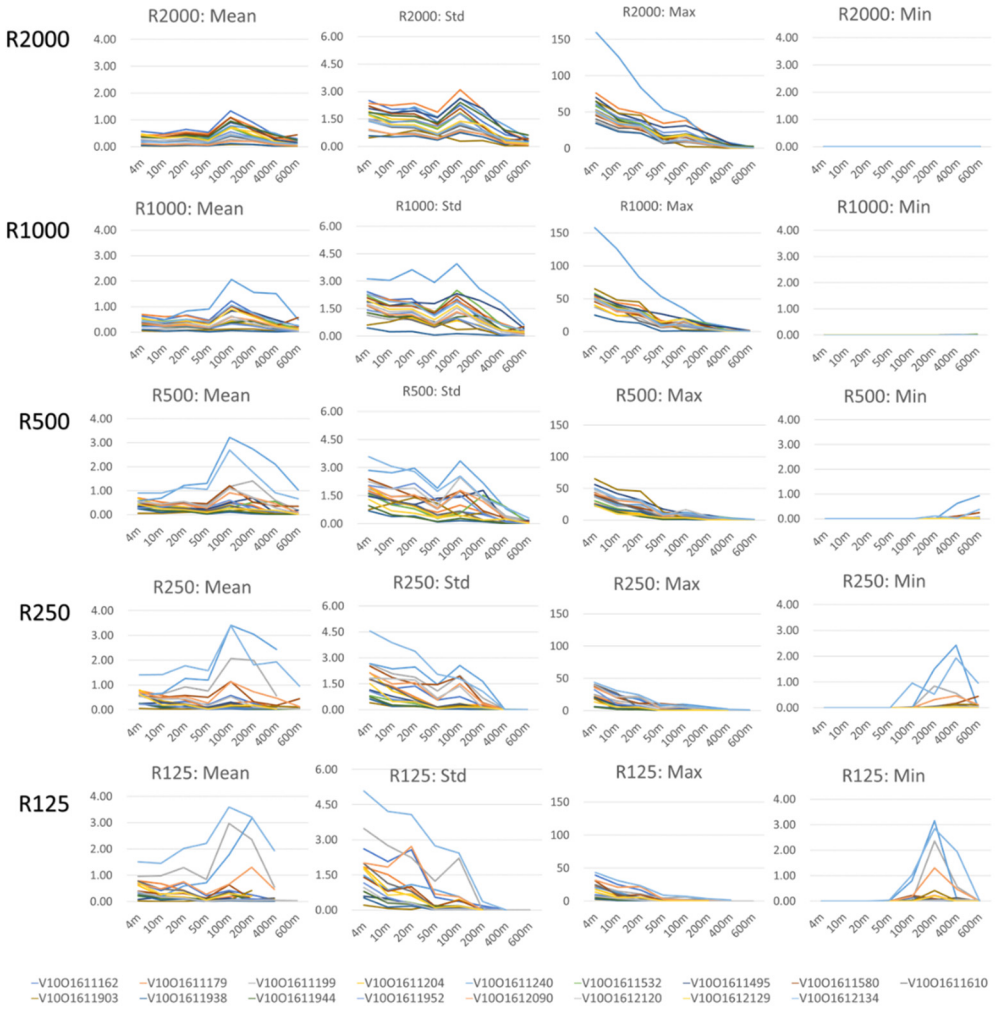


Figure 10. Variations in the statistical mean, max, and std of Mac_{z0} for the 17 AWSs, according to eight grid sizes (4, 10, 25, 50, 100, 200, 400, and 600 m) and five search radii (2000, 1000, 500, 250, and 125 m, denoted as R2000, R1000, R500, R250, and R125, respectively).

Table 6. Average AT, RH, and difference in z_0 values (E–W vs. N–S wind directions) for the 17 AWSs.

AWS ID	AWS Measurements		z_0 Difference for Different Averaging Circles (radii)				
	AT	RH	2000 m	1000 m	500 m	250 m	125 m
V10O1611532	24.28	65.80	−0.73	−0.61	−0.39	−0.29	−0.15
V10O1611903	25.39	73.98	−0.14	−0.21	−0.30	−0.05	−0.03
V10O1611938	26.33	65.78	−0.11	−0.08	−0.17	−0.15	−0.11

Table 6. *Cont.*

AWS ID	AWS Measurements		z_0 Difference for Different Averaging Circles (radii)				
	AT	RH	2000 m	1000 m	500 m	250 m	125 m
V10O1611580	26.36	65.17	−1.16	−1.08	−1.16	−1.34	−1.00
V10O1611199	26.50	62.05	−0.25	−0.37	−0.85	−1.49	−1.66
V10O1611162	26.60	62.82	−1.64	−1.59	−0.74	−0.45	−0.51
V10O1612120	26.74	61.41	−0.44	−0.64	−1.07	−0.60	−0.28
V10O1612129	26.82	60.90	−0.71	−0.82	−0.28	−0.20	−0.32
V10O1611952	27.10	62.28	−0.49	−0.40	−0.75	−0.31	−0.32
V10O1611179	27.17	59.65	−0.87	−0.87	−0.74	−0.82	−0.92
V10O1611610	27.46	59.82	−0.35	−0.45	−0.56	−0.50	−0.86
V10O1611495	27.47	58.86	−0.65	−0.87	−0.47	−0.18	−0.23
V10O1611944	27.54	62.43	−0.78	−0.39	−0.23	−0.18	−0.25
V10O1612090	27.60	60.98	−0.21	−0.62	−0.76	−0.99	−0.88
V10O1611204	27.68	59.53	−0.68	−0.53	−0.63	−0.63	−0.54

4. Discussion

The lack of ground truth data and underdeveloped application methods will continue to increase the need for a multi-scale approach to explore urban aerodynamic roughness. However, the proposed morphologic methodology and its outputs can help provide a better understanding of the impact of current building placement on urban aerodynamic roughness. However, many assumptions and limitations have impacted previous studies; thus, determining wind-friendly placements or shapes of buildings is difficult [7,10,11,17–19]. Further research is needed to provide information on urban building morphology management and its benefits [8,15,16]. Therefore, this section focuses on three parts: (1) Morphometric Method: Quantifying Urban Building Placement, (2) Observational Method: Verification of Urban Climate Influence, and (3) Future RS Research: Supporting Building Placement Management.

4.1. Morphometric Method: Urban Building Placement Quantificatoin

After reviewing the z_0 and related UCPs obtained from LiDAR 3DPC analyses, we believe that some of the multi-scale urban aerodynamic roughness exploration goals have been achieved. The main factors that have been appropriately quantified and explored are detailed below.

(1) Quantification of current urban building placements using LiDAR 3DPC: this study developed a GUI to perform a thorough morphometric analysis of urban building placements using the LiDAR 3DPC database. Contemporary PC computing power, coupled with GUI workbenches, can efficiently process a large volume of 3DPC files and generate various UCPs at multiple resolutions (ranging from a few meters to hundreds of meters) within a matter of days. Furthermore, as all data are provided in geographical coordinates, users and experts can share their data and rapidly communicate for more sustainable urban aerodynamic roughness. For instance, the tool can provide a basis for ensuring granularity while considering the demand for rapid data production and sharing to initiate land use management discussions, as shown in high-rise residential land-use zones (UQA123, Table 5).

(2) Experimental test for building aerodynamic roughness using LiDAR 3DPC: estimation methods and various grid sizes can be applied to test two wind directions (Figure 5). Although we did not adjust the building shapes or placements in this study, designers or planners can use their designs or plans as 3DPC inputs to determine whether their changes might affect urban aerodynamic roughness. Notably, many UQA123 areas in

the study region remain undeveloped (Figure 8a) and could be an interesting building placement planning study testbed for developing a better urban morphometric roughness form.

(3) Exploration of multi-scale urban aerodynamic roughness: urban buildings are being constructed rapidly, and their placements change both horizontally and vertically. LiDAR technology is a good choice for such explorations due to its detailed surveys and easy automation. As shown in Figure 5c, the results from multi-scale exploration provide new insights into the complexity of urban building settings, the immature state of morphometric methods, and the lack of ground truth data. Nonetheless, the need for multi-scale urban aerodynamic roughness studies will increase, not only for quantification purposes but also for the development of qualitative methods that can reveal unnoticed information through improved visual interpretation.

Additional tasks must also be accomplished to realize practical evidence-based utilization of building placement management, such as urban planning or urban design. The main morphometric quantification issues and limitations are as follows.

(1) Immature applicational conceptualization for public contribution: The concepts and benefits of managing mean urban wind through building placement are not well known; hence, the analysis and utilization of mean urban wind are not widely accepted by the public. However, individual building-related concepts that can improve the management of gusty winds caused by high-rise buildings have been well documented. This conceptually contradicts mean urban wind management, as it considers only the building and neighboring space. The field of numerical modeling offers several approaches to enhance the forecasting of flash rains or floods through detailed modeling of the vertical behavior of urban winds induced by high-rise buildings [12–14]. Therefore, it is imperative to strengthen the conceptualization of mean wind management [7] according to evidence-based data collection and analysis [11,13,41] to reduce contradictions and enhance collaboration.

(2) Technically immature GUI: This issue limits sufficient morphometric simulations of urban planning or design perspectives, not only from an 'as-is' standpoint but also from a 'to-be' perspective. Regarding the 'as-is' standpoint, the GUI results are inferior in terms of the initial configuration of urban prevailing wind. Currently, only two wind directions (N–S and E–W) can be applied, although the prevailing wind direction can vary by site. Additionally, the logic underlying the identification of urban prevailing winds is unclear. Considering the influence of prevailing wind direction on morphometric quantification, synoptic wind directions and local wind directions must be considered. Furthermore, the logic should be developed to enhance the reliability of morphometric quantification. For the 'to-be' perspective, future building construction or urban placement change plans should integrate LiDAR 3DPCS data into GUI functionality to support various land-use stakeholders through application and dissemination. The current methodology is overly focused on weather prediction, and a methodological fusion with other disciplines is necessary. For instance, the Computational Fluid Dynamics (CFD) modeling approach supports various types of urban building management through physics-based simulation [12,42]. However, the CFD model has limitations in supporting urban-scale wide and providing detailed high-resolution outputs in a timely manner due to its extensive computing resource requirements [42]. Although the proposed methodological application is in its infancy, it has the potential to mature with CFD approaches. It can support outputs that cover an entire urban area in detail while consuming fewer computing resources and less time. Hence, a combined approach that exploits the advantages of both methods should be considered.

4.2. Observational Method: Verification of Urban Climate Influence

Despite significant advancements in weather observation technology, novel observational methods are needed to verify the effects of building placement on wind or climate because both are invisible. Several observational studies, such as BUBBLE, have attempted to validate urban wind patterns by installing dense tall towers and instrumentation for monitoring [43]. However, field observational data collection ceased after the project concluded. Collecting dense observational data for large-scale urban areas using state-of-the-art instruments such as flux towers is currently unrealistic, mainly due to cost constraints. While this study generated abundant multi-scale data, strict validation using observational methods is impractical due to high costs and spatial limitations associated with installing tall towers and instrumentation.

Therefore, the development of cheaper, more practical, and reliable validation methods should be considered over scientifically accurate but expensive or infeasible methods [41]. Two approaches have been actively discussed to address these issues: validation using less-accurate but low-cost instruments [44–46] and validation using virtual instrumentation [47–50].

This study introduces the first approach because reducing manufacturing costs accelerates dissemination and widens the range of applications, not only for weather phenomena such as wind but also for air quality factors such as particulate matter (PM) and nitrogen dioxide (NO2) [41,46]. Although the proposed approach has not been fully disseminated, its widespread use is feasible due to technological advancements and ease of reinstallation or relocation. While wind observations were not feasible, we discovered a stronger relationship between RH and z_0 than between AT and z_0. The relationships between z_0 and various environmental factors will soon be verifiable using this inexpensive measurement approach. However, experience and knowledge on its utilization are currently insufficient. Notably, a stick design and installation-based data collection method are necessary to enhance the reliability of observational evidence.

The second approach is also being actively discussed for the digital twinning of the environment for prediction and management purposes [20]. From a virtual validation perspective, it should not be viewed as a substitute for physically instrumented observational validation but rather as an extensive virtual validation sensor, which needs to be evaluated as a more expansive and practically feasible solution. Its methodological sources vary and include numerical simulations, such as CFD, but also satellite remote sensing and even inexpensive measurement data, as discussed for the first approach [41,44–46]. The accelerating trend of digitalization is blurring the boundary between real and virtual validations. However, the dissemination of the second approach may not be faster than that of the first approach because validation from the first approach is required.

4.3. Future RS Research: Building Placement Management Support

In South Korea, high-rise residential apartments are emerging as a dominant form of housing [40], and this trend is spreading to the surrounding urban areas. Thus, high-rise building cluster landscapes and the aerodynamic roughness of residential areas in downtown regions will likely change dramatically. If we do not prepare wind-friendly plans, relevant management indicators, and affordable data-model tools, then new buildings in undeveloped areas, such as the UQA123 zone (Figure 8a), will not represent an improvement relative to existing modern architecture.

Figure 11 depicts typical urban land use views constructed from various building coverage ratios (BCRs) and floor area ratios (FARs) corresponding to each land use management category and desired designs. Notably, in South Korea, the BCR and FAR effectively force specific building forms (Figure 11a and 11b) [51]. Therefore, to apply wind-friendly design principles (Figure 11c) to undeveloped areas, BCRs and FARs related to incentives or regulation tools should be linked to the z_0 of measured relevant attributes.

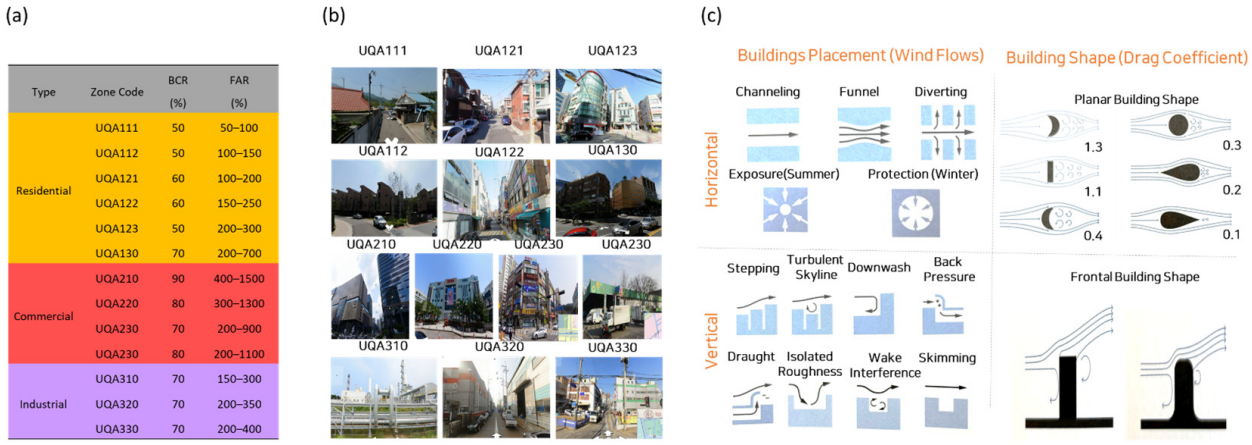


Figure 11. Casual urban scenery forced based on BCR and FAR regulations and desirable wind-friendly designs. (**a**) BCR and FAR for each land-use zone in South Korea; (**b**) street view scenery (source: Google Street); and (**c**) horizontal and vertical buildings design components and drag coefficients [52].

However, before connecting land use regulations or building codes with urban building placement principles, societal attitudes towards an ecologically sustainable and wind-friendly urban future must change [20,52,53]. To date, significant research has been performed, such as planning potential air pathways to promote fresh-air flow [15,16,18], planning supportable, rapid and integrated approaches [54–56], promoting legislation for housing and urban sector energy efficiency [20,57], and developing instrumental architect design principles [52,58]. However, if each discipline is not integrated to realize an ecologically sustainable and wind-friendly development, then the urban future may resemble Yang's description of the built environment [53,58]:

> 'The built environment no matter how well designed will intrude, displace spatially, and alter the ecology of the ecosystem on which it is located by its physical presence'.

According to Yang's theoretical framework for urban built environment ecological transition, a new positive cycle has developed between the man-made environment and natural ecosystems (see Figure 12). While LiDAR RS research addresses urban atmospheric processes, RS shows considerable potential to provide both quantitative information and qualitative knowledge, thus fostering a transition from the micro- to macro-scale [59,60].

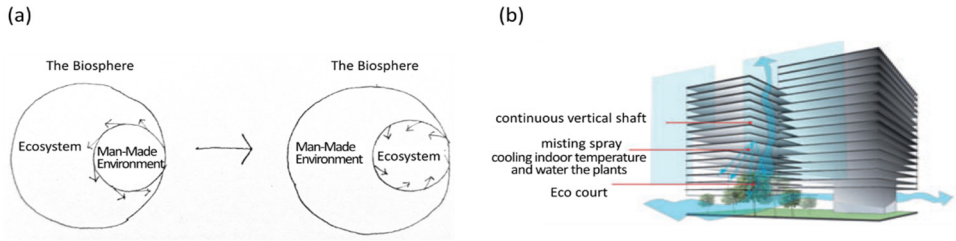


Figure 12. (**a**) Biosphere diagram for a new positive cycle between the man-made environment and natural ecosystems [53], and (**b**) architectural concept ecoskyscraper design [58].

5. Conclusions

This study investigated the influence of building placement on urban aerodynamic roughness using airborne LiDAR 3DPC analysis. The multi-scale exploration results demonstrate both the potential of this approach and its limitations, thus highlighting the need for further research. The conclusions are as follows.

First, the application of LiDAR 3DPC for multi-scale explorations of aerodynamic roughness is feasible. This method provides a means to address the differences in urban building configuration data with various spatial resolutions. Further studies should focus on expanding morphological applications and disseminating the findings.

Second, validation methods that rely on expensive equipment are not practical for this approach. Instead, emerging cost-effective observation or virtual sensor techniques are more feasible and practical for dissemination.

Third, current regulations such as BCR and FAR should be linked to z_0 to apply the study's findings to new residential areas. Moreover, additional RS research is needed to generate more quantitative information and qualitative knowledge.

Author Contributions: Writing, S.M.A.; software, B.K.; validation, C.Y.; supervision, J.-H.E., J.-H.W. and W.W.; funding acquisition, J.-H.W. and C.Y. All authors have read and agreed to the published version of the manuscript.

Funding: This research was funded by the Korea Meteorological Administration Research and Development Program under grant KMI (KMI2021-03312) and funded by Korea Environment Industry & Technology Institute (KEITI) through Climate Change R&D Project for New Climate Regime., funded by Korea Ministry of Environment (MOE) (RS-2022-KE002096).

Data Availability Statement: To use LiDAR data for evaluation purposes, contact the Smart Spatial Information Divi-sion, NGII (Email: ngii2018@korea.kr, Tel: +82-31-210-2700). For use of AWS data, visit the Air-MapKorea website (https://iot.airmapkorea.kt.com/info/, accessed on 26 June 2024).

Conflicts of Interest: Author B. Kim was employed by the company TENELEVEN Inc. The remaining authors declare that their research was conducted without any commercial or financial relationships that could be seen as potential conflicts of interest.

References

1. Riffat, S.; Powell, R.; Aydin, D. Future cities and environmental sustainability. *Future Cities Environ.* **2016**, *2*, 1. [CrossRef]
2. Güneralp, B.; Reba, M.; Hales, B.U.; Wentz, E.A.; Seto, K.C. Trends in urban land expansion, density, and land transitions from 1970 to 2010: A global synthesis. *Environ. Res. Lett.* **2020**, *15*, 044015. [CrossRef]
3. Wiedmann, T.; Allen, C. City footprints and SDGs provide untapped potential for assessing city sustainability. *Nat. Commun.* **2021**, *12*, 3758. [CrossRef] [PubMed]
4. Crompvoets, J.; Vancauwenberghe, G.; Ho, S.; Masser, I.; De Vries, W.T. Governance of national spatial data infrastructures in Europe. *Int. J. Spat. Data Infrastruct. Res.* **2018**, *13*, 253–285. [CrossRef]
5. Ching, J.; Mills, G.; Bechtel, B.; See, L.; Feddema, J.; Wang, X.; Ren, C.; Brousse, O.; Martilli, A.; Neophytou, M.; et al. WUDAPT: An urban weather, climate, and environmental modeling infrastructure for the Anthropocene. *Bull. Amer. Meteor. Soc.* **2018**, *99*, 1907–1924. [CrossRef]
6. Wellinger, N.; Gubler, M.; Müller, F.; Brönnimann, S. GIS-based revision of a WUDAPT Local Climate Zones map of Bern, Switzerland. *City Environ. Interact.* **2024**, *21*, 100135. [CrossRef]
7. Coceal, O.; Belcher, S.E. Mean winds through an inhomogeneous urban canopy. *Bound.-Layer Meteorol.* **2005**, *115*, 47–68. [CrossRef]
8. Mills, G. Luke Howard and the climate of London. *Weather* **2008**, *63*, 153–157. [CrossRef]
9. Hebbert, M.; Jankovic, V. Cities and climate change: The precedents and why they matter. *Urban Stud.* **2013**, *50*, 1332–1347. [CrossRef]
10. Grimmond, C.S.B.; Oke, T.R. Aerodynamic properties of urban areas derived from analysis of surface form. *J. Appl. Meteorol. Climatol.* **1999**, *38*, 1262–1292. [CrossRef]
11. Kent, C.W.; Grimmond, S.; Gatey, D. Aerodynamic roughness parameters in cities: Inclusion of vegetation. *J. Wind Eng. Ind. Aerodyn.* **2017**, *169*, 168–176. [CrossRef]
12. Scherer, D.; Antretter, F.; Bender, S.; Cortekar, J.; Emeis, S.; Fehrenbach, U.; Gross, G.; Halbig, G.; Hasse, J.; Maronga, B.; et al. Urban climate under change [UC] 2—A national research programme for developing a building-resolving atmospheric model for entire city regions. *Meteorol. Z.* **2019**, *28*, 95–104. [CrossRef]
13. Mendis, P.; Ngo, T.; Haritos, N.; Hira, A.; Samali, B.; Cheung, J. Wind loading on tall buildings. *Electron. J. Struct. Eng.* **2007**, *7*, 41–54. [CrossRef]
14. Kim, D.J.; Kang, G.; Kim, D.Y.; Kim, J.J. Characteristics of LDAPS-predicted surface wind speed and temperature at automated weather stations with different surrounding land cover and topography in Korea. *Atmosphere* **2020**, *11*, 1224. [CrossRef]
15. Ren, C.; Ng, E.Y.Y.; Katzschner, L. Urban climatic map studies: A review. *Int. J. Climatol.* **2011**, *31*, 2213–2233. [CrossRef]
16. Acero, J.A.; Kupski, S.; Arrizabalaga, J.; Katzschner, L. Urban climate multi-scale modelling in Bilbao (Spain): A review. *Procedia Eng.* **2015**, *115*, 3–11. [CrossRef]

17. Huang, M.; Liu, D.; Weng, H.; Hong, C.; Tao, Z.; Huang, Y. Size effect of anisotropic rock joint with two-order roughness. *Geomech. Geophys. Geo-Energy Geo-Resour.* **2023**, *9*, 8. [CrossRef]
18. Gál, T.; Unger, J. Detection of ventilation paths using high-resolution roughness parameter mapping in a large urban area. *Build. Environ.* **2009**, *44*, 198–206. [CrossRef]
19. Yi, C.; Kwon, T.H.; Park, M.S.; Choi, Y.J.; An, S.M. A study on the roughness length spatial distribution in relation to the Seoul building morphology. *Atmosphere* **2015**, *25*, 339–351. [CrossRef]
20. An, S.M.; An, Y.H.; Kim, I.H. *A Study on Digital Twinning Applications for a Land Use with Wind*; Korea Research Institute for Human Settlements: Sejong, Republic of Korea, 2021; Volume 21, pp. 19–21. Available online: https://www.krihs.re.kr/ (accessed on 26 June 2024).
21. Kim, D.H.; Hong, S.O.; Byon, J.Y.; Park, H.; Ha, J.C. Development and evaluation of urban canopy model based on Unified Model input data using urban building information data in Seoul. *Atmosphere* **2019**, *29*, 417–427. [CrossRef]
22. An, S.M.; Kim, D.H.; Hong, S.O.; Jae-Yong, B. A fundamental study for urban canopy layer analysis and application: Focusing on Seoul Metropolitan Area urban weather service domain. *Korea Spat. Plan. Rev.* **2020**, *105*, 101–120. [CrossRef]
23. Yan, W.Y.; Shaker, A.; El-Ashmawy, N. Urban land cover classification using airborne LiDAR data: A review. *Remote Sens. Environ.* **2015**, *158*, 295–310. [CrossRef]
24. Yi, C.; An, S.M. A study on building identification from the three-dimensional point cloud by using Monte Carlo integration method. *J. Korean Assoc. Geogr. Inf. Stud.* **2020**, *23*, 16–41. [CrossRef]
25. An, S.M. A study on urban-scale building, tree canopy footprint identification and sky view factor analysis with airborne lidar remote sensing data. *Remote Sen.* **2023**, *15*, 3910. [CrossRef]
26. Wang, J.; Bretz, M.; Dewan, M.A.A.; Delavar, M.A. Machine learning in modelling land-use and land cover-change (LULCC): Current status, challenges and prospects. *Sci. Total Environ.* **2022**, *822*, 153559. [CrossRef] [PubMed]
27. Lettau, H. Note on aerodynamic roughness-parameter estimation on the basis of roughness-element description. *J. Appl. Meteorol.* **1969**, *8*, 828–832. [CrossRef]
28. Macdonald, R.W.; Griffiths, R.F.; Hall, D.J. An improved method for the estimation of surface roughness of obstacle arrays. *Atmos. Environ.* **1998**, *32*, 1857–1864. [CrossRef]
29. Yi, C.; Yang, H. Heat Exposure information at screen level for an impact-based forecasting and warning service for heat-wave disasters. *Atmosphere* **2020**, *11*, 920. [CrossRef]
30. NGII. Geospatial Information Hub of Korea National Geographic Information Institute. Available online: https://www.ngii.go.kr/lib/file/pr_02.pdf (accessed on 26 June 2024).
31. Raupach, M.R. Simplified expressions for vegetation roughness length and zero-plane displacement as functions of canopy height and area index. *Bound.-Layer Meteorol.* **1994**, *71*, 211–216. [CrossRef]
32. Bottema, M.; Mestayer, P.G. Urban roughness mapping–validation techniques and some first results. *J. Wind Eng. Ind. Aerodyn.* **1998**, *74–76*, 163–173. [CrossRef]
33. Kanda, M.; Inagaki, A.; Miyamoto, T.; Gryschka, M.; Raasch, S. A new aerodynamic parametrization for real urban surfaces. *Bound.-Layer Meteorol.* **2013**, *148*, 357–377. [CrossRef]
34. Dolman, A.J. Estimates of roughness length and zero plane displacement for a foliated and non-foliated oak canopy. *Agric. For. Meteorol.* **1986**, *36*, 241–248. [CrossRef]
35. Raupach, M.R. Drag and drag partition on rough surfaces. *Bound.-Layer Meteorol.* **1992**, *60*, 375–395. [CrossRef]
36. Korean Law Information Center. Available online: https://www.law.go.kr/lsSc.do?section=&menuId=1&subMenuId=15&tabMenuId=81&eventGubun=060101&query=%EC%B4%88%EA%B3%A0%EC%B8%B5%EA%B1%B4%EB%AC%BC#undefined (accessed on 26 June 2024).
37. Dalheimer, M. *Programming with QT: Writing portable GUI applications on Unix and Win32*; O'Reilly Media, Inc.: Newton, MA, USA, 2002.
38. American Society for Photogrammetry & Remote Sensing (ASPRS). *LAS Specification 1.4-R15*; ASPRS: Bethesda, MD, USA, 2009. Available online: https://www.asprs.org/ (accessed on 26 June 2024).
39. Farkas, G. Possibilities of using raster data in client-side web maps. *Trans. GIS* **2020**, *24*, 72–84. [CrossRef]
40. Oppenheim, R. On the republic of apartments. *East Asian Sci. Technol. Soc.* **2009**, *3*, 137–145. [CrossRef]
41. Woo, J.H.; An, S.M.; Hong, K.; Kim, J.J.; Lim, S.B.; Kim, H.S.; Eum, J.H. Integration of CFD-Based Virtual Sensors to A Ubiquitous Sensor Network to Support Micro-Scale Air Quality Management. *J. Environ. Inform.* **2016**, *27*, 85–97. [CrossRef]
42. Kim, J.J.; Baik, J.J. Effects of street-bottom and building-roof heating on flow in three-dimensional street canyons. *Adv. Atmos. Sci.* **2010**, *27*, 513–527. [CrossRef]
43. Rotach, M.W.; Vogt, R.; Bernhofer, C.; Batchvarova, E.; Christen, A.; Clappier, A.; Feddersen, B.; Gryning, S.E.; Martucci, G.; Mayer, H.; et al. BUBBLE–an urban boundary layer meteorology project. *Theor. Appl. Climatol.* **2005**, *81*, 231–261. [CrossRef]
44. Carotta, M.C.; Martinelli, G.; Crema, L.; Malagù, C.; Merli, M.; Ghiotti, G.; Traversa, E. Nanostructured thick-film gas sensors for atmospheric pollutant monitoring: Quantitative analysis on field tests. *Sens. Actuators B Chem.* **2001**, *76*, 336–342. [CrossRef]
45. Hart, J.K.; Martinez, K. Environmental sensor networks: A revolution in the earth system science? *Earth-Sci. Rev.* **2006**, *78*, 177–191. [CrossRef]
46. Castell, N.; Dauge, F.R.; Schneider, P.; Vogt, M.; Lerner, U.; Fishbain, B.; Bartonova, A. Can commercial low-cost sensor platforms contribute to air quality monitoring and exposure estimates? *Environ. Int.* **2017**, *99*, 293–302. [CrossRef]

47. Liu, L.; Kuo, S.M.; Zhou, M. Virtual sensing techniques and their applications. In Proceedings of the International Conference on Networking, Sensing and Control, Okayama, Japan, 26–29 March 2009; pp. 31–36. [CrossRef]
48. Hill, D.J.; Liu, Y.; Marini, L.; Kooper, R.; Rodriguez, A.; Futrelle, J.; McLaren, T. A virtual sensor system for user-generated, real-time environmental data products. *Environ. Model. Soft.* **2011**, *26*, 1710–1724. [CrossRef]
49. Lin, Z.; Wang, X.; Yuan, J.; Gui, Y. Virtual Reality-Based Digital Landscape Experience and Climate Change Monitoring: Evidence from Human Thermal Comfort. *Sustainability* **2024**, *16*, 4366. [CrossRef]
50. Yeang, K. A Theoretical Framework for the Incorporation of Ecological Considerations in the Design and Planning of the Built Environment. Ph.D. Dissertation, Cambridge University Library, Cambridge, UK, 1981.
51. OECD. *The Governance of Land Use in Korea Urban Regeneration*; OECD Publishing: Washington, DC, USA, 2019. [CrossRef]
52. Krautheim, M.; Pasel, R.; Pfeiffer, S.; Schultz-Granberg, J. *City and Wind: Climate as an Architectural Instrument*; DOM Publishers: Berlin, Germany, 2014.
53. Ibelings, H. *Modern Architecture: A Planetary Warming History*; The Architecture Observer: Amsterdam, The Netherlands, 2023.
54. Ng, E. Policies and technical guidelines for urban planning of high-density cities–air ventilation assessment (AVA) of Hong Kong. *Build. Environ.* **2009**, *44*, 1478–1488. [CrossRef] [PubMed]
55. Li, Z.; Wang, Z.; Wu, L.; Huang, W.; Peng, W. Evaluating the effect of building patterns on urban flooding based on a boosted regression tree: A case study of Beijing, China. *Hydrol. Process.* **2023**, *37*, e14932. [CrossRef]
56. Huang, Y.; Lin, J.; He, X.; Lin, Z.; Wu, Z.; Zhang, X. Assessing the scale effect of urban vertical patterns on urban waterlogging: An empirical study in Shenzhen. *Environ. Impact Assess. Rev.* **2024**, *106*, 107486. [CrossRef]
57. Wende, W.; Huelsmann, W.; Marty, M.; Penn-Bressel, G.; Bobylev, N. Climate protection and compact urban structures in spatial planning and local construction plans in Germany. *Land Use Policy* **2010**, *27*, 864–868. [CrossRef]
58. Yeang, K.; Powell, R. Designing the ecoskyscraper: Premises for tall building design. *Struct. Des. Tall Build.* **2007**, *16*, 411–427. [CrossRef]
59. Wang, Z.; Menenti, M. Challenges and opportunities in Lidar remote sensing. *Front. Remote Sens.* **2021**, *2*, 641723. [CrossRef]
60. Wentz, E.A.; Anderson, S.; Fragkias, M.; Netzband, M.; Mesev, V.; Myint, S.W.; Seto, K.C. Supporting global environmental change research: A review of trends and knowledge gaps in urban remote sensing. *Remote Sens.* **2014**, *6*, 3879–3905. [CrossRef]

Disclaimer/Publisher's Note: The statements, opinions and data contained in all publications are solely those of the individual author(s) and contributor(s) and not of MDPI and/or the editor(s). MDPI and/or the editor(s) disclaim responsibility for any injury to people or property resulting from any ideas, methods, instructions or products referred to in the content.